# Functional Analysis of Neurons in the Chick Spinal Accessory Lobes

（ニワトリ脊髄アクセサリーローブ内のニューロンにおける機能的検討）

2011

Yuko Yamanaka

The United Graduate School of Veterinary Science,

Yamaguchi University

## CONTENTS

## PREFACE

Posture and locomotion in vertebrates are controlled by a variety of motor centers in the brain and spinal cord. To cope with environmental and internal demands, these motor centers are supplied with information from all sensory systems [35]. Most vertebrae walk using their forelimbs and hindlimbs, i.e. they do quadrupedalism. On the other hand, birds have two different types of locomotion. One is flying using their forelimbs and the other is bipedal walking using their hindlimbs. It has been suggested for long time that a special balance-sensing organ of the body is necessary for birds during walking on the ground, because their hindlinmbs are located at the rear of the gravity center, and some lines of evidence supported this idea [3, 7]. At present, the proposed location of such an organ is the lumbosacral region of the vertebrae [32].

In vertebrates, neuronal somata are mainly located in the grey matter of the spinal cord. However, the somata of paragriseal neurons are present also in the spinal white matter of many vertebrates [37]. In the avian spinal cord, ten pairs of protrusions, called accessory lobes (ALs), are present at both lateral sides of the lumbosacral spinal cord near the dentate ligaments [38]. In addition to scattered paragriseal cells in the white

matter of the spinal cord, histological results haves shown that neurons gather in the ALs to construct the major marginal nuclei of Hofmann [2, 21]. The majority of cells in the AL are glycogen-rich glial cells (glycogen cells). Somata of the paragriseal neurons are scattered in a pool of AL glycogen cells and these neurons have been reported to show some morphological properties as a mechanoreceptive neurons [37, 38]. In birds, the vertebrae are fused at the lumbosacral region. However, the borders of the vertebrae are left and construct bilateral grooves on the inner surface of the dorsal wall of the vertebral canals. The ventral ends of these grooves are covering the ALs. Such construction built by the ALs and the grooves resembles the construction of the semicircular canals in the inner ear [27, 32] (Fig. 1A, quoted from Necker, 2006, and Fig. 1B). This morphological and histological information suggests that ALs act as a sensory organ and have a role in keeping the body balance in combination with the vertebral canals during walking on the ground [28]. In fact, behavioral experiments have shown that destruction of the lumbosacral vertebral canal disturbed bipedal walking of pigeons [31].

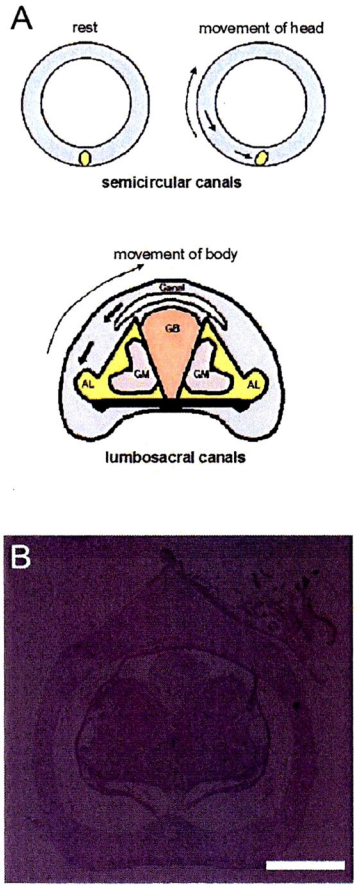


**Fig. 1.** (A) Scheme of the possible function of the lumbosacral canals (bottom) as compared to the function of the semicircular canals (top). Movements of the head result in an inertia-driven bending of the cupula (yellow oval) which excites the sensory hair cells whose stereocilia reach into the cupula. Similarly, during rotations of the body inertia of the fluid in the lumbosacral canals and near the accessory lobes (AL) is thought to mechanically distort the lobes, which then results in a mechanical stimulation and excitation of the finger-like processes of the lobe neurons. (B) Transverse section of the lumbosacral vertebral column of a chick at the level of the glycogen body. H.E. stain. AL: accessory lobe, GB: glycogen body, GM: gray matter. Scale bars: 1 mm.

# CHAPTER 1

Chick spinal accessory lobes contain functional neurons expressing voltage-gated sodium channels to generate action potentials

# INTRODUCTION

Although there have been much experimental evidence to suggest that ALs in birds act as the sensory organ, there is little cellular evidence to indicate that a cell in AL has a neuronal function and it is unknown whether AL cells functionally express voltage-gated ion channels to generate action potentials. In Chapter 1, to elucidate these points, we developed a method to dissociate cells from chick ALs and made electrophysiological recordings in acutely isolated AL cells.

## MATERIALS AND METHODS

*Cell preparation*

Preparation of AL neurons was made from Chick embryo at embryological stages ranging E14–E18. The lumbosacral vertebral column was dissected from chick embryo. A spinal cord containing the lumber enlargement and the glycogen body was removed from the vertebra (Fig. 2-1A). Ten pairs of ALs were found at both lateral sides of the lumbosacral spinal cord (Fig. 2-1A, B). ALs numbered #2 to #8 in Fig. 2-1A and B were carefully dissected from the spinal cord with micro scissors under the stereomicroscope (Fig. 2-1C). Collected ALs were stored in ice-cold $Ca^{2+}$-free HEPES-buffered solution (CFHBS), containing 154 NaCl, 6 KCl, 1.2 $MgCl_2$, 10 Glucose, 10 HEPES (in mM); pH was adjusted to 7.4 with NaOH, and 0.2% bovine serum albumin (Sigma, St Louis, MO, USA). ALs were rinsed with fresh CFHBS three times and were stored in 100% $O_2$-gassed CFHBS supplemented with 0.1% Trypsin (Invitrogen, Carlsbad, CA, USA) on ice for 20 min. Subsequently, the tissues were gently triturated with a fire-polished and silicon-coated pasteur pipettes. Trypsin solution, in which ALs sank, were gassed with 100% $O_2$ again and ALs were incubated at 37°C for 20 min with mechanical

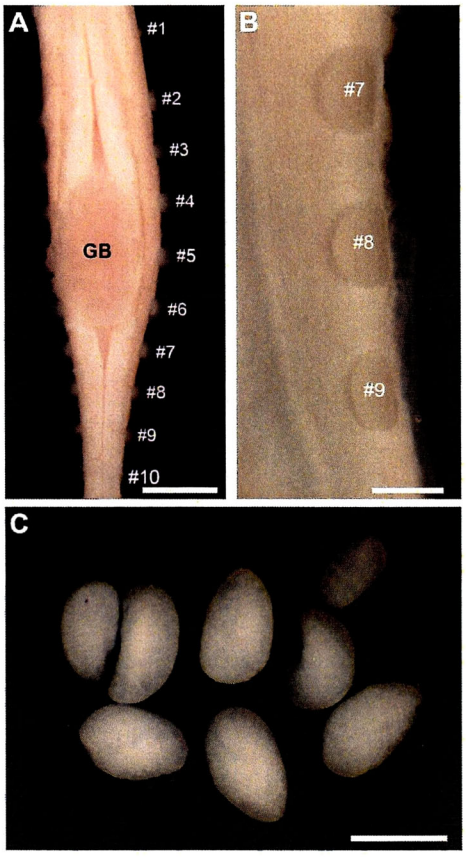


**Fig. 2-1.** Spinal ALs of the chick and dissociated cells. Cells were isolated from ALs located at the lumbosacral spinal cord of the chick at E18. (A) The chick spinal cord at the lumbosacral region. Glycogen body (GB) on the dorsal surface and ten pairs (numbered #1-#10) of ALs at both lateral sides of the spinal cord are found. (B) An enlargement of ALs numbered #7-#9 at the right side. (C) Mechanically dissected ALs from the spinal cord. Scale bars: A, 2 mm; B, C, 500 μm

shaking at 100 rpm to accelerate an enzymatic digestion. The tissues were cooled on ice for 1 min, and were gently triturated by pipetting with the pasteur pipettes. Three pasteur pipettes with decreasing tip bore sizes, approximately 0.5-1 mm in diameter, were used. Tissues were triturated by 20-stroke pipetting with each pipette (totally 60 strokes). This procedure usually resulted in complete digestion of AL tissues from 1 embryo. After the mechanical digestion, cell suspension was centrifuged (500 x g, 10 min at 4°C) and pellets were resuspended in CFHBS to remove the enzyme. This cetrifugation-resuspension procedure was repeated twice, and dissociated cells were plated on round glass coverslips coated with Cell-Tak™ (Becton Dickinson, Franklin Lakes, NJ, USA) and were used in the following experiments.

*Electrophysiology*

Whole-cell currents and membrane potentials were measured with standard whole-cell voltage clamp and current clamp techniques, respectively. Recording pipettes were pulled from micro glass capillaries (GD-1.5, Narishige, Tokyo, Japan) by the framed puller (P-97, Sutter, Novato, CA, USA). The pipettes with 2.5-4 MΩ tip

resistance were used. The normal bath solution contained (in mM): 144 NaCl, 10 NaOH, 6 KCl, 2.5 $CaCl_2$, 1.2 $MgCl_2$, 10 HEPES, 10 Glucose, and was adjusted to pH 7.4 with HCl. In the experiment to examine voltage-current relationship of an inward current that was consisted mainly by voltage-gated $Na^+$ current ($I_{NaV}$), $Na^+$ concentration in the bath solution was decreased to 40 mM by isotonic replacement of $Na^+$ with $NMDG^+$ (40Na solution). TTX, (Wako Pure Chemical, Osaka, Japan) was added to the bath solution from the concentrated stock solution. Cells were continuously perfused with the bath solutions at a flow rate of 1 ml/mim by the gravity and the overflowed solution was vacuumed by an electronic pump. The pipette solution contained (in mM): 145 K-Methansulfonate (Ms), 3.4 KCl, 6 NaMs, 2 $MgCl_2$, 1.3 $CaCl_2$, 10 Glucose, 10 EGTA, 10 HEPES, and was adjusted pH 7.4 with Ms ($K^+$-rich pipette solution). The free $Ca^{2+}$ concentration in the pipette solution was calculated to be $10^{-8}$ M (Max Chelator Software, Stanford University). In experiments to examine voltage-current relationship of the inward current, $K^+$ in the pipette solution was removed by isotonic replacement with $Cs^+$ ($Cs^+$-rich pipette solution). An agar bridge containing 2% agar and 154-mM NaCl in conjunction with Ag-AgCl wire was used as the reference electrode. Because

liquid-junction potentials between every bath and every pipette solutions were measured to be less than ±3 mV, they were not corrected. The patch-clamp amplifier used was EPC10 (HEKA, Lambrecht/Pfalz, Germany). Whole-cell current and potential signals were measured and membrane potentials and currents were controlled by Patch Master software (HEKA) running on Macintosh (Apple, Cupertino, CA, USA). All electrophysiological experiments were done at room temperature (24–26°C). Stored data were analyzed by Igor Pro software (WaveMetrics, Lake Oswego, OR, USA). Data are presented mean ± SEM ($n$ = the number of observation).

## RESULTS

*Morphological features of dissociated accessory lobe cells*

Cell suspension prepared from chick AL tissues contained mainly two types of cells. One had round shape with clear cytosol and sometimes had short dendrites (Fig. 2-2A). The other had also round shape with rich cytosolic structures and often several dendrites and/or axons with many branches (Fig. 2-2B). Both types of cells had similar size. The diameters of the cell body of cells with the clear cytosol and with the rich cytosolic structures were 13.9 ± 0.64 μm (n = 20) and 18.8 ± 0.47 μm ($n$ = 39), respectively.

*Cell-physiological features of dissociated accessory lobe cells*

Whole-cell currents were measured from both types of the cells dialyzed with the $K^+$-rich pipette solution and perfused with the normal bath solution containing 154-mM $Na^+$. The cells were voltage clamped at a holding potential of –80 mV. After waiting cell dialysis with the pipette solution (at least 2 min), 50-ms voltage pulses to the levels between –90 mV and +20 mV with 10-mV step were applied with 5-s intervals (Fig. 2-3A). From the cells with the clear cytosol, no voltage-gated current was observed (Fig. 2-3B). On the other hand, from the cells with the rich cytosolic structures, rapidly activating and inactivating inward currents were consistently observed by voltage pulses

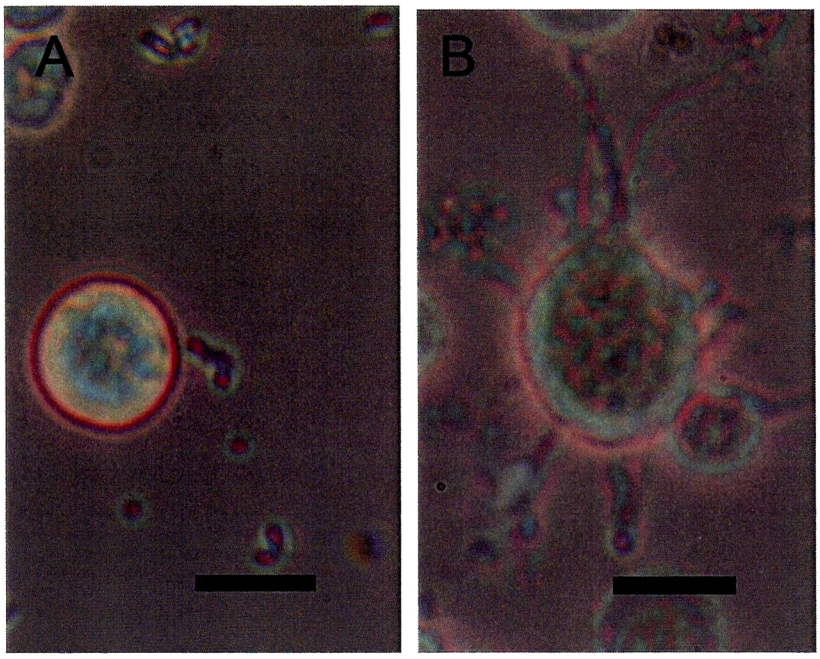


**Fig. 2-2.** A typical cell with a round shape and clear cytosol (A) and a typical cell with rich cytosolic structures and processes (B) isolated from ALs by the enzymatic digestion. Scale bars: A, B 20 μm.

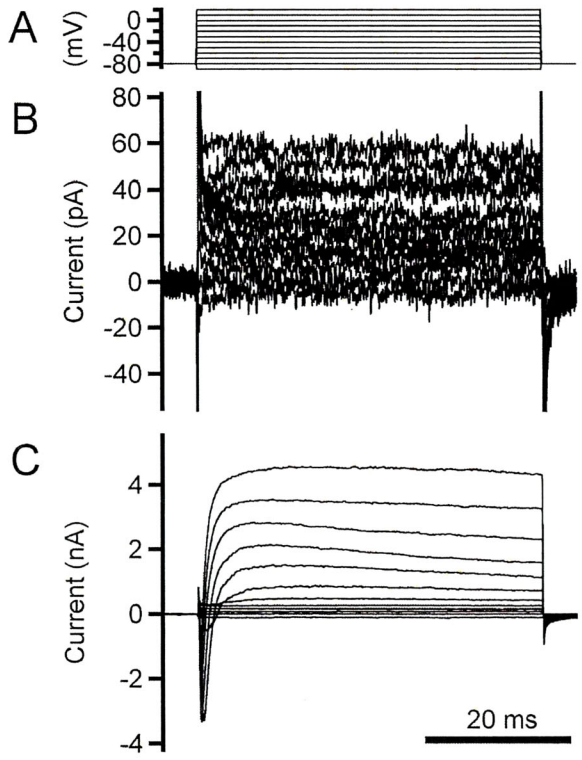


**Fig. 2-3.** Voltage-dependent current responses in a dissociated AL cell. (A) Series of voltage pulses from the holding potential of –80 mV to the potentials between –90 and +10 mV were applied. (B, C) Typical current responses to voltage pulses in the whole-cell voltage clamp configuration in the cell with clear cytosol (B) and the rich cytosolic structures (C). The cell were dialyzed with the $K^+$-rich pipette solution and perfused with the normal bath solution containing 154-mM $Na^+$.

to more depolarized potentials than –40 mV and slowly activated outward currents were observed by the voltage pulses to more depolarized potentials than –30 mV (Fig. 2-4). The membrane capacitance of cells with the rich cytosolic structures was 13.6 ± 1.20 pF ($n$ = 27). Typical current responses in such a cell are shown in Fig. 2-3C. Inward and outward currents resembled $I_{NaV}$ and voltage-gated $K^+$ currents ($I_{KV}$) commonly seen in mammalian neurons, respectively. In addition, some cells with the rich cytosolic structures showed slowly activating and inactivating inward currents in response to depolarizing by voltage pulses. Typical current responses in such a cell are shown in Fig. 2-5. These inward currents resembled voltage-gated $Ca^{2+}$ currents ($I_{CaV}$) commonly seen in mammalian neurons. Subsequently, membrane potentials were recorded in the current clamp mode. Under the condition with the $K^+$-rich pipette solution and the normal bath solution, a resting membrane potential was –57.8 ± 1.82 mV ($n$ = 9). Increasing amplitudes of depolarizing currents were injected to cells and responded changes in membrane potentials were recorded (Fig. 2-6A, B). The current injection inducing depolarization to potentials more depolarized than –40 mV caused rapid depolarization reaching +30 mV followed by rapid repolarization. Similar results were obtained from more than 9 independent cells.

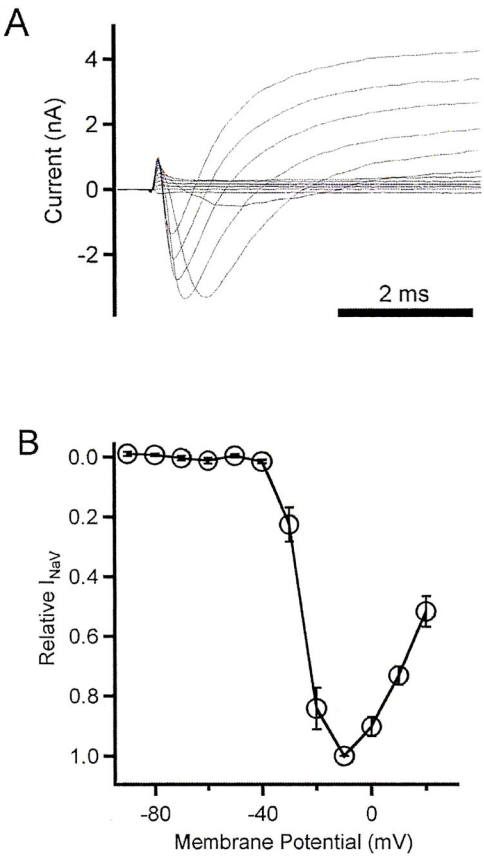


**Fig. 2-4.** A voltage-current relationship of the inward current. (A) Series of voltage pulses from the holding potential of –80 mV to the potentials between –90 and +10 mV were applied. Typical current responses to voltage pulses in the whole-cell voltage clamp configuration in a cell with rich cytosolic structures. The cell was dialyzed with the $K^+$-rich pipette solution and perfused with the normal bath solution containing 154-mM $Na^+$. (B) Summarized voltage-current relationship of the inward current in 5 cells. Normalized amplitudes of the inward currents were plotted against the potentials of applied pulses. The current amplitudes were normalized by that obtained at –10 mV in each cell.

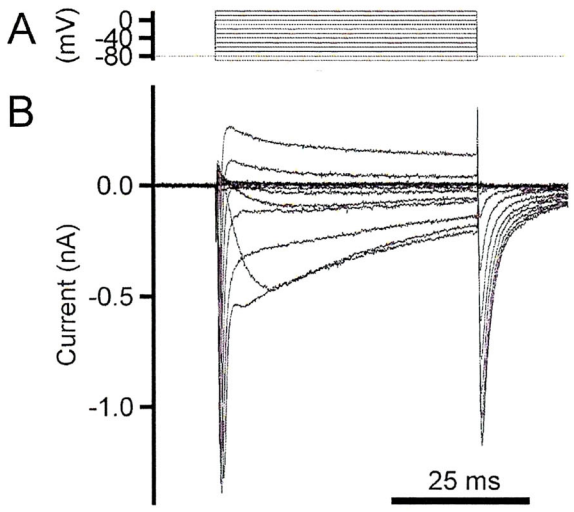


**Fig.2-5.** Voltage-gated $Ca^{2+}$ current ($I_{CaV}$)-like currents in a dissociated AL cell. (A) Series of voltage pulses from the holding potential of –80 mV to the potentials between –90 and +10 mV were applied. (B) Typical current responses to voltage pulses in the whole-cell voltage clamp configuration in a cell with the rich cytosolic structures. The cell was dialyzed with the $K^+$-rich pipette solution and perfused with the normal bath solution containing 154-mM $Na^+$. The cells showed not only rapidly activating and inactivating inward currents but also slowly activating and inactivating inward currents in response to the voltage pulses.

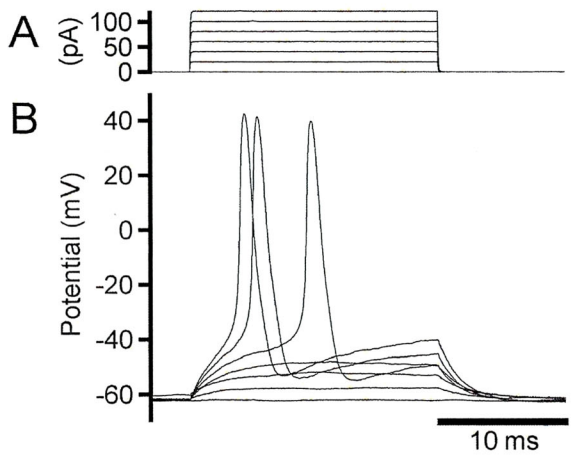


**Fig. 2-6.** Voltage-dependent potential responses in a dissociated AL cell. (A) Series of current pulses with 20-pA steps were applied. (B) Typical membrane potential responses to current injection in the whole-cell current clamp configuration in the same cell in Fig. 2-3C.

*Effect of TTX on inward currents in accessory lobe neurons*

To confirm whether activation of voltage-gated $Na^+$ channel (VGSC) caused the rapid inward current, effects of TTX on the inward current responded to depolarization were examined. TTX at 100 nM was applied to the bath solution, and the series of the voltage pulses were applied to the cells before, during and after the application of TTX (Fig. 2-7A). TTX reversibly inhibited the inward currents with no effect on the outward currents. Similar results were obtained from 4 other cells, and the peak amplitudes of the rapidly activating inward current evoked by the depolarization pulses to –10 mV were inhibited by TTX (100 nM) by 85.1 ± 3.6% ($n$ = 5, Fig. 2-7B).

*Activation and inactivation of the voltage-gated $Na^+$ channel in accessory lobe neurons*

To assess the voltage-current relationship of the rapidly activating and inactivating inward current, the cells were dialyzed with the $Cs^+$-rich pipette solution and the depolarizing pulses were applied. In these cells, the outward currents were drastically decreased (Fig. 2-8A, B). The amplitudes of the depolarization-evoked inward currents were decreased by an extracellular perfusion with 40Na solution (Fig. 2-9A, B). Under this condition, the series of the voltage pulses were applied. In the presence of 154-mM $Na^+$, huge inward currents, sometimes reaching 10 nA, were observed in response to the

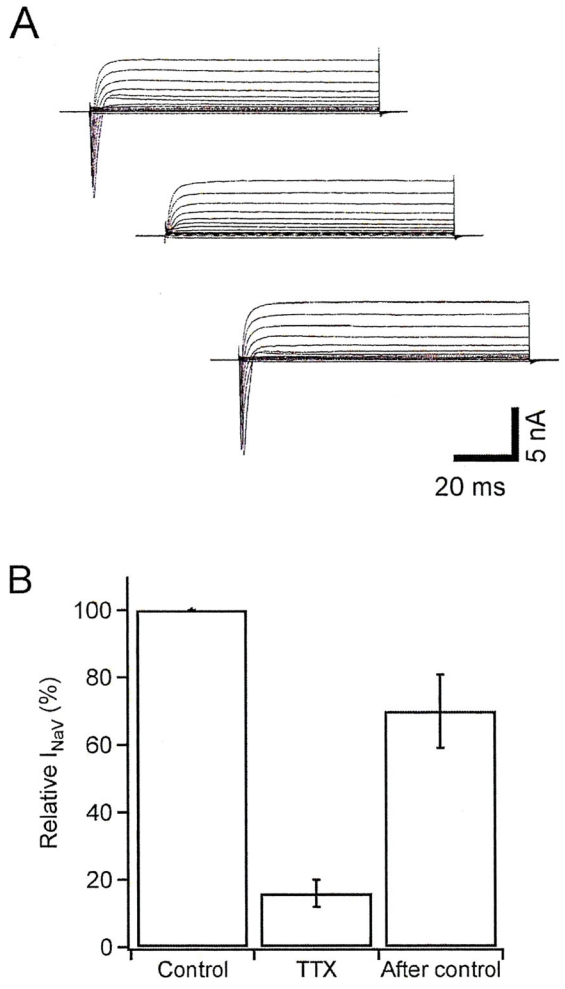


**Fig. 2-7.** Effect of TTX on voltage-gated current in a dissociated AL cell. (A) Typical current responses are shown. The cell was dialyzed with the $K^+$-rich pipette solution and perfused with the normal bath solution containing 154-mM $Na^+$. Series of voltage pulses from the holding potential of –80 mV to the potentials between –90 and +10 mV were applied before (control), during (TTX) and after (after control) the application of 100-nM TTX. (B) Effects of TTX ($n = 4$) on inward currents are summarized. The columns and bars indicate the relatice $I_{NaV}$ before, during and after the application of TTX.

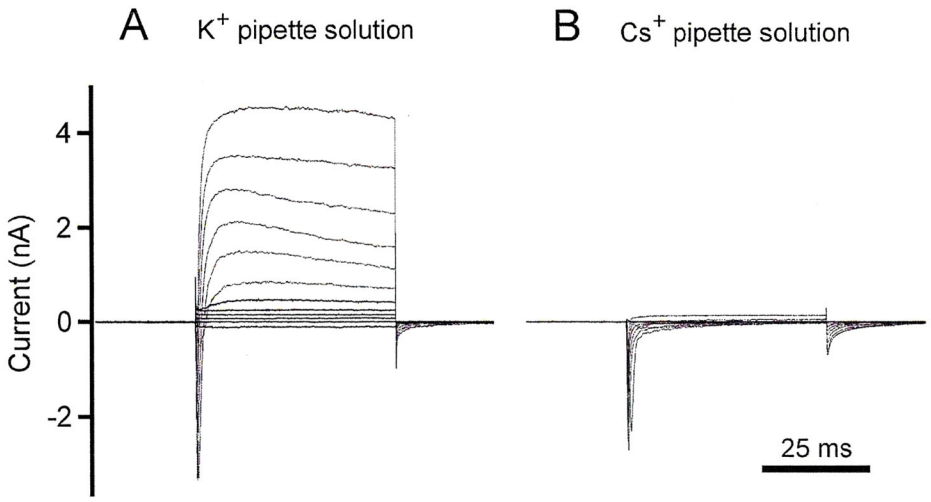


**Fig. 2-8.** Comparison between voltage-dependent current responses in cells dialyzed with the $K^+$-rich pipette solution and $Cs^+$-rich pipette solution. (A, B) Typical current responses to voltage pulses in the whole-cell voltage clamp configuration. Series of voltage pulses from the holding potential of –80 mV to the potentials between –90 and +10 mV for 50 ms were applied to cells perfused with the normal bath solution containing 154-mM $Na^+$. The cells were dialyzed with the $K^+$-rich pipette solution (A) or the $Cs^+$-rich pipette solution (B).

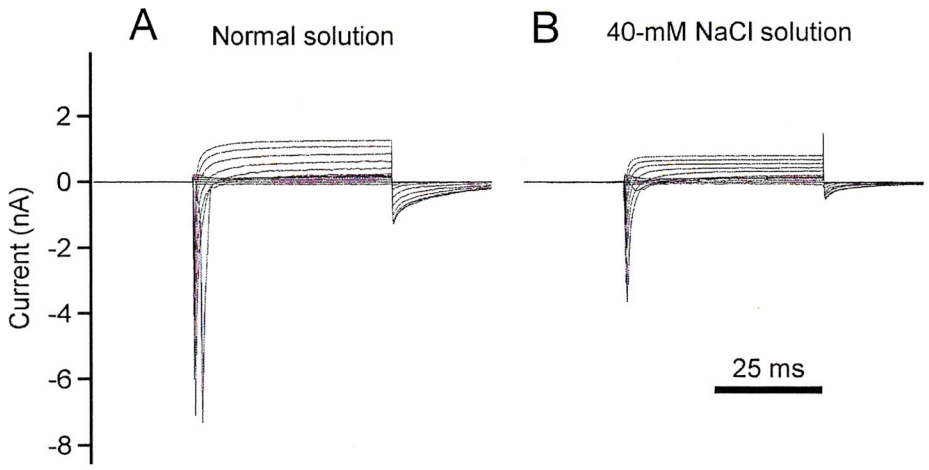


**Fig. 2-9.** Comparison between voltage-dependent current responses in cells perfused with the normal bath solution containing 154-mM $Na^+$ and 40Na solution containing 40-mM $Na^+$. (A, B) Typical current responses to voltage pulses in the whole-cell voltage clamp configuration. Series of voltage pulses from the holding potential of –80 mV to the potentials between –90 and +10 mV for 50 ms were applied to the cell dialyzed with the $Cs^+$-rich pipette solution. The cell was perfused with the normal bath solution containing 154-mM $Na^+$ (A) or 40Na solution (B).

depolarizing voltage steps. Because such huge inward currents caused critical errors in the clamping voltage, the properties of the inward currents were assessed in the presence of 40Na solution. The inward currents measured in the presence of 40Na solution and the $Cs^+$-rich pipette solution also showed rapidly activating and inactivating kinetics. The amplitudes of the inward currents at each test pulse potential were quantified by measuring differences between the peak amplitudes of the inward currents and the leak current levels that were calculated by the linear regression of the leak currents at –90, –80 and –70 mV. The normalized amplitudes of the inward current were plotted against the potentials of the applied pulses (Fig. 2-10). The inward current was observed in response to the pulses to more depolarized potentials than –50 mV and reached maximum at –10 mV. In the experiments using the pulses to more depolarized potentials, the amplitudes of the inward currents decreased with increase in the test pulse potentials. Time to peak of the inward current and the time constants of current decay were determined by analyzing the current responses to the voltage pulse at –10 mV. Time to peak was 0.56 ± 0.063 ms ($n$ = 19, Fig. 2-11). Time course of decay was fitted with a double exponential function expressing: $I(t) = I_{fast}$ x $\exp(-t/\tau_{fast}) + I_{slow}$ x $\exp(-t/\tau_{slow})$, where $I_{fast}$ and $I_{slow}$ are amplitudes of fast and slow components of total inward current, and $\tau_{fast}$ and$\tau_{slow}$ are time constants of decay (Fig. 2-12). The estimated

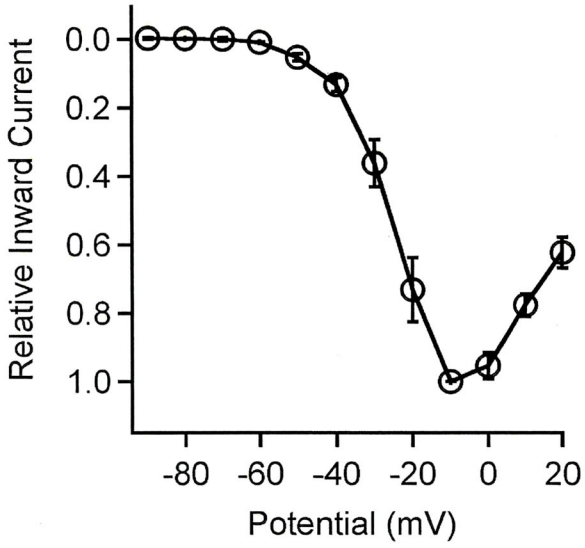


**Fig. 2-10.** Summarized voltage-current relationship of the inward current in 5 cells. Normalized amplitudes of the inward current were plotted against the potentials of applied pulses. The current amplitudes were normalized by that obtained at –10 mV in each cell. The cell was dialyzed with the $Cs^+$-rich pipette solution and perfused with 40Na solution.

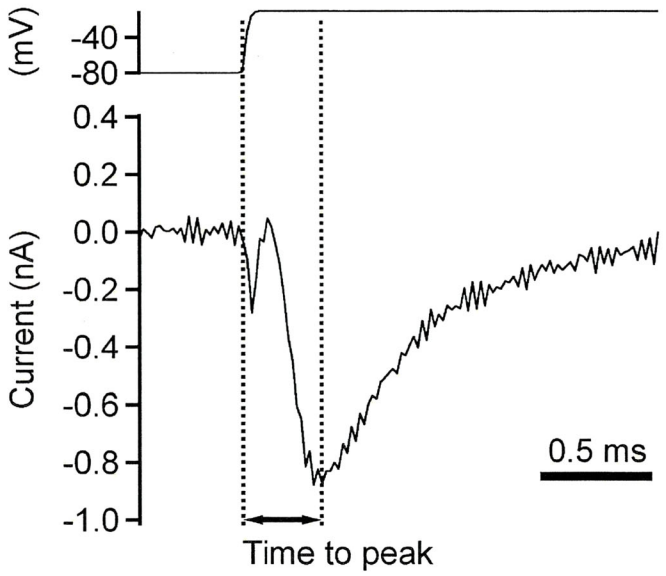


**Fig. 2-11.** Kinetics in activation of the inward currents. "Time to peak" was defined as an interval form beginning of the voltage pulse at –10 mV to peak of the inward currents. Typical traces of changes in holding potential (*upper trace*) and membrane currents (*lower trace*) are shown, respectively.

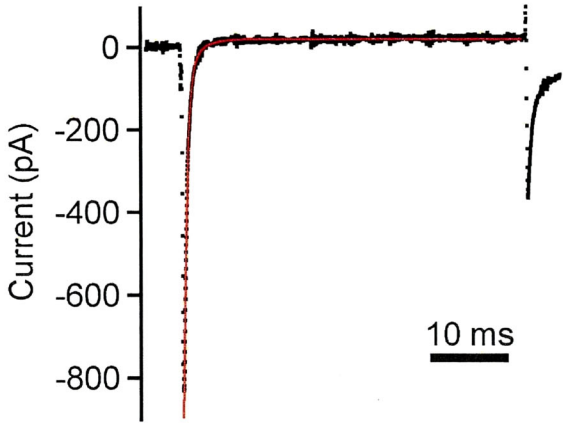


**Fig. 2-12.** Kinetics in inactivation of the inward currents. A typical example of time course of decay fitted with a double exponential function fitting (*red line*).

$\tau_{fast}$ and $\tau_{slow}$ were 0.68 ± 0.05 ms and 12.1 ± 2.3 ms, respectively ($n$ = 19).

Similarly to the analysis of voltage-dependent activation of the inward currents, the inactivation properties were also analyzed. To examine voltage dependence of the inactivation of the inward currents, the double pulse protocol consisting of a 50-ms test pulse to –10 mV proceeded by a 50-ms conditioning pulse to various potentials ranging between –90 mV and –10 mV from the holding potential of –80 mV was utilized (Fig. 2-13). As seen in Fig. 2-8B and 2-13B, in the cells dialyzed with the $Cs^+$-rich pipette solution and perfused with 40Na solution, the outward currents evoked by depolarization remained. To minimize the influence of the outward current on the voltage-inactivation relationship, the amplitudes of the rapidly inactivating current were measured by subtracting the inactivated levels during 50-ms test pulses from the peak levels in each current response. The amplitudes of the inward current at –10 mV were decreased by the conditioning pulses to more depolarized potentials than –70 mV and mostly inactivated by those to –20 mV (*closed symbols* in Fig. 2-14). The voltage-inactivation relationship was fitted with the Boltzmann function expressing: $I(V_m) = I_{max}/\{1 + \exp[(V_m - V_{half})/k]\}$, where $I_{max}$ is the maximal activation of the inward currents elicited by the test pulse to +10 mV, $V_m$ is the potential of the applied pulse, $V_{half}$ is the potential of the pulse to induce half inactivation, and $k$ is the slope

factor. The estimated $V_{half}$ and $k$ were –43.3 ± 1.8 mV and –5.6 ± 0.33 mV ($n$ = 6), respectively.

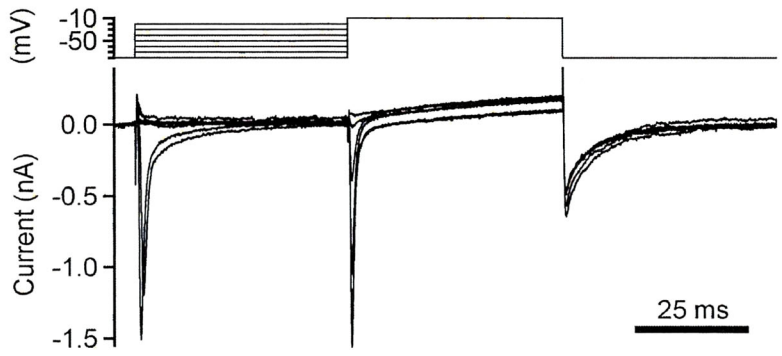


**Fig. 2-13.** Inactivation of the rapidly activating inward current in an AL cell. Typical current responses (*lower traces*) obtained with a double pulse protocol in the whole-cell voltage clamp configuration. Test pulses to –10 mV for 50 ms proceeded by a 50-ms conditioning pulse to various potentials ranging between –90 mV and –10 mV from the holding potential of –80 mV were applied (*upper traces*). The cell was dialyzed with the $Cs^+$-rich pipette solution and perfused with 40Na solution.

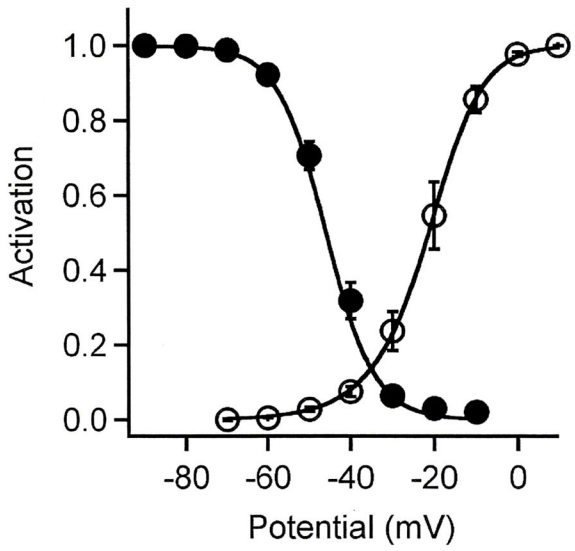


**Fig. 2-14.** Summarized activation (*open circles*, $n = 5$) and inactivation (*closed circles*, $n = 6$) curves of the rapidly activating inward current in AL cells. Activation of the inward current was assessed by dividing the current amplitudes by driving force for $Na^+$ based on the calculated reversal potential (+49 mV) and normalizing by the maximum current. Inactivation of the inward current was assessed by dividing the amplitudes of the test pulse-evoked inward current by those with the conditioning pulses to –90 mV in each cell and normalized by the maximum current. Lines show the regression curves of averaged values fitted by the Boltzmann function.

## DISCUSSION

*Comparisons of morphological and cell-physiological characters*

In the cells that had the rich cytosolic structures and were perfused with 154-mM $Na^+$-containing solution, the amplitudes of the rapidly activating and inactivating inward currents varied from 0.8 nA to 5 nA independent of apparent sizes of somata. TTX at 100 nM inhibited more than 85% of the inward currents. The remaining inward current in the presence of 100-nM TTX could be $I_{NaV}$ through TTX-sensitive VGSCs that were not blocked by 100-nM TTX or $I_{NaV}$ through TTX-resistant VGSCs. They could also be $Ca^{2+}$ currents through voltage-gated $Ca^{2+}$ channels, since $I_{CaV}$ –like inward currents were observed in some AL neurons. Any way, the effect of TTX indicates that majority of the channel types causing the rapidly activating and inactivating inward currents in chick AL cells are TTX-sensitive VGSCs.

Outward currents were clearly smaller in neurons dialyzed with the $Cs^+$-rich solution than currents obtained with the $K^+$-rich pipette solution, indicating that these outward currents are carried by $K^+$ through voltage-gated $K^+$ channels, which are commonly seen in mammalian excitable cells. In the cells dialyzed with the $Cs^+$-rich pipette solution and perfused with 40Na solution, the outward currents evoked by depolarization were drastically decreased, but remaining outward currents were detected.

The voltage-current relationship of the depolarization-evoked inward currents resembles that of current through VGSC in mammalian cells. This result is consistent with the conclusion that the major type of channels causing the rapid inward currents is TTX-sensitive VGSC in chick AL cells. Therefore, the activation curve of the rapidly activating and inactivating inward current in consideration of driving force for $Na^+$ was calculated (*closed symbols* in Fig. 2-14). The voltage-activation relationship was fitted with the Boltzmann function expressing: $I(V_m) = I_{max}/\{1 + \exp[(V_m - V_{half})/k]\}$, where $I_{max}$ is the maximal activation of the inward current elicited by the test pulse to +10 mV, $V_m$ is the potential of the applied pulse, $V_{half}$ is the potential of the pulse to induce half activation of the inward current, and $k$ is the slope factor. The estimated $V_{half}$ was –17.1 ± 1.6 mV and $k$ was 5.3 ± 0.97 mV ($n$ = 5). The voltage-dependent inactivation of the inward current was also observed. The activation and the inactivation kinetics of the inward current at –10 mV and the voltage dependence of the activation and the inactivation are consistent with those of fast inactivating and TTX-sensitive VGSCs found in mammalian cells [41, 42].

Considering that AL consists of glycogen cells and neurons [28, 37, 38], the dissociated cells with the clear cytosol and no voltage-gated ionic currents may be the glycogen cells derived from the astroglial cells. In contrast, the other type of cells with

the rich cytosolic structures showed voltage-gated currents, indicating that they express functional VGSCs and voltage-gated $K^+$ channels. Moreover, these cells generate complete action potentials. These results clearly indicate that the cells with the rich cytosolic structures are functional neurons. This conclusion is also supported by the observation of the morphology of the dissociated cells. The acutely dissociated chick AL cells with the clear cytoplasm sometimes had short processes, and the cells with the rich cytosolic structures sometimes had some dendrites or axons with many branches. Such morphology is consistent with the reported properties of the glycogen cells and neurons in pigeon ALs, respectively [38].

*Ability of accessory lobe neurons*

It has been proposed that AL neurons function as sensory neurons of equilibrium [32]. However, there is little information about the activity of VGSC and the action potential in avian sensory neurons. Recently, the properties of $I_{NaV}$ in vestibular hair cells of the embryo and adult chick have been reported [23]. In vestibular hair cells in embryo, small amplitudes of $I_{NaV}$ were recorded and the amplitude increased during development. However, even in the hair cells of the adult chick, depolarizing current injection caused only action potential-like response reaching –20 mV under the

current-clamped condition. They seem to be unable to generate the complete action potentials. It is not the same case in AL neurons in embryo chick. AL neurons can generate the complete action potentials, which closely resembles propagating action potentials observed in mammalian neurons.

The complete action potentials recorded in the current clamp mode under the whole-cell configuration suggest that AL neurons can propagate the action potential along the axon toward the synaptic terminal located far from the soma, and that they can make the functional projection to other neurons. It has been reported that AL neurons extend axons projecting to lamina VIII neurons in the contralateral spinal gray matter [10, 32], which project to the contralateral ventral horn motoneurons in the pigeons [32]. There is little information about functional roles of lamina VIII neurons of birds. Assuming that their functional roles are same as those of mammals [4, 15, 16], they may have a role in motor coordination of right and left hindlimbs. Therefore, it is reasonable to propose that AL neurons send the sensory information to lamina VIII neurons. The functional evidence in the present study in addition to the morphological [10, 30] and the behavioral evidence [34] supports this proposal.

# CHAPTER 2

Analysis of GABA-induced inhibition of spontaneous firing

in chick accessory lobe neurons

## INTRODUCTION

Electrophysiological experiments *in vivo* have shown that vibration applied to the body of pigeons evoked electrical activity of ALs, and most AL neurons showed spontaneous activities in the absence of the vibratory stimuli [29]. In addition to the results and other reports for ALs, we show that ALs contain functional neurons using the whole-cell patch clamp technique in Chapter 1 [45]. However, it was unclear whether isolated AL neurons have intrinsic mechanism to exhibit spontaneous activity like hair cell afferents of the vestibular semicircular canal.

Based on the immunohistochemical experiments, it has been reported that AL neurons have several neurotransmitters and their receptors [25, 28]. For example, the outer layer of AL neurons shows consistently γ-aminobutyric acid (GABA)- and glutamic acid decarboxylase (GAD)-like immunoreactivity. On the other hand, centrally located neurons did not show GABA and GAD-like immunoreactivity, but were surrounded by distinct GABA- and GAD-positive nerve terminals.

However, there has been no report to show spontaneous activity at cell physiological level and a physiological function of GABA in AL neurons to date. In the present study, we investigate presence of spontaneous activity in isolated AL neurons and effects of GABA, a most abundant inhibitory neurotransmitter in central nerve system, on

electrical activity of AL neurons using the patch clamp technique.

## MATERIALS AND METHODS

*Cell preparation*

The lumbosacral vertebral column was dissected and the spinal cord containing the lumbar enlargement and the glycogen body was removed from the vertebra. ALs were carefully dissected from the spinal cord with micro scissors under a stereomicroscope. Collected ALs were stored in Hanks's Balanced Salt Solution (HBSS), containing 5.4 KCl, 0.44 $KH_2PO_4$, 4.2 $NaHCO_3$, 137 NaCl, 0.33 $NaH_2PO_4$, 5.5 glucose, 0.05 Phenol Red Sodium Salt (in mM), and 0.2% bovine serum albumin (Sigma, St Louis, MO, USA). ALs were rinsed with fresh HBSS three times and were stored in HBSS. HBSS supplemented with 1unit/ml papain (Worthington, New Jersey, USA) and L-cysteine hydrochloride (Sigma) was pre-incubated at 37°C for 15 min with mechanical shanking at 100 rpm to activate the enzyme. Subsequently, AL tissues were transferred to the papain solution and incubated at 37 °C for 5 min with mechanical shanking at 100 rpm. After the enzymatic treatment, Dulbecco's Modified Eagle Medium (D-MEM) was added to the papain solution to stop enzyme activity. AL tissues were gently triturated by pipetting with Pasteur pipettes. Three Pasteur pipettes with decreasing tip bore sizes, approximately 0.5-1 mm in diameter, were used. Tissues were triturated by 5 strokes of pipetting with each pipette (total of 15 strokes). This procedure usually resulted in

complete digestion of AL tissues from 2 embryos. After the mechanical trituration, cell suspension was centrifuged (500×g, 10 min at 4 °C) and a pellet was resuspended in D-MEM to remove the enzyme. This centrifugation-resuspension procedure was repeated twice, and dissociated cells were plated on round glass coverslips coated with Cell-Tak™ (Becton Dickinson, Franklin Lakes, NJ, USA) The cells were maintained under the standard culture condition and were used in the following experiments within 6 h from the isolation.

*Electrophysiology*

Spontaneous spike activity was recorded in the on-cell patch clamp configuration. Whole-cell currents and membrane potentials were recorded by the standard whole-cell technique in the voltage clamp and current clamp modes, respectively. Recording pipettes were pulled from micro glass capillaries (GD-1.5, Narishige, Tokyo, Japan) by a framed puller (P-97, Sutter, Novato, CA, USA). The pipettes with 2.5-5 MΩ tip resistance were used. The normal bath solution contained (in mM): 154 NaCl, 6 KCl, 2.5 $CaCl_2$, 1.2 $MgCl_2$, 10 HEPES, 10 glucose, and was adjusted to pH 7.4 with tris(hydroxymethyl)aminomethane (Tris) and the N-Methyl-D-glutamine (NMDG)-Cl bath solutions contained (in mM): 165 NMDG-Cl, 10 HEPES, 10 glucose, and was

adjusted to pH 7.4 with Tris. Cells were continuously perfused with the bath solutions at a flow rate of 1 ml/min by gravity and the overflowed solution was vacuumed by an electronic pump. In the standard whole-cell recording, pipettes were filled with the KCl-rich pipette solution (mM): 123 KCl, 10 EGTA-2K, 6 NaCl, 1.3 $CaCl_2$, 2 ATP-Mg, 0.3 GTP-Na, 10 HEPES, 10 glucose and adjusted pH at 7.4 with Tris. In the experiments with ramp commands in the whole-cell configuration and the gramicidin-perforated recording, pipettes were filled with the CsCl-rich pipette solution (mM): 130 CsCl, 10 EGTA-2Cs, 1.3 $CaCl_2$, 2.0 $MgCl_2$, 10 HEPES, 10 glucose and adjusted pH at 7.4 with Tris.

A physiological intracellular concentration of $Cl^-$ ($[Cl^-]_i$) was examined by the gramicidin-perforated recordings. These experiments were made using the same pipettes as used in the experiment with ramp commands. Gramicidin (Sigma) was dissolved in methanol at 10 mg/ml. Subsequently, the gramicidin solution was added to the CsCl-rich pipette solution to give a final gramicidin concentration at 0.1 mg/ml. Pipettes were tip-filled with the gramicidin-free pipette solution and then back-filled with the gramicidin-containing solution. Once a giga ohm seal was established, neurons were held until a series resistance reached a stabilized level at smaller than 50 MΩ. Usually, it took 25-40 min after contact of the pipette tips to the neurons. An agar bridge

containing 2% agar and 154-mM NaCl in conjunction with an Ag-AgCl wire was used as a reference electrode. Since liquid-junction potentials between bath and pipette solutions were measured as being smaller than ± 3 mV, they were not corrected. The patch-clamp amplifier used was EPC-10 (HEKA, Lambrecht/Pfalz, Germany). Currents and potentials were controlled and measured by Patch Master software (HEKA) running on Macintosh (Apple, Cupertino, CA, USA). All electrophysiological experiments were performed at room temperature (24-26 °C). Stored data were analyzed off-line by IGOR Pro software (WaveMetrics, Lake Oswego, OR, USA).

*Drugs*

The following drugs were dissolved in distilled water and stored at –20 °C. Concentrations of the stock solutions are as follows: tetrodotoxin (TTX, Waco Pure Chemical, Osaka, Japan); 1 mM, GABA (Sigma); 100 mM, muscimol (Sigma); 50 mM, SKF97541 (Alexis Biochemicals, Lausenne, Switzerland); 50 mM, bicuculline (Sigma); 10 mM, CGP35348 (Sigma); 10 mM.

*Data acquisition and statistical analysis*

Spontaneous spike activity was analyzed from typical records during 2-3 min period.

The spike frequency was calculated as an inverse of a mean interspike interval (ISI). The coefficient of variation (CV) was calculated in the same records as used to calculate spike frequencies ($n = 36$). The CV was defined as the standard deviation (SD) of the ISI divided by the mean of the ISI. Effects of GABA and its agonists on spontaneous spike activities were analyzed by comparing spike frequencies during longer than 5-s periods in the presence of the agonists with those during 20-s periods showed stable spikes before and after the application of the agonists. In all experiments in this study, GABA and GABA receptor agonists were applied until electrical activities of the AL neurons reached steady or peak levels. When inhibition of spontaneous spike activities or GABA-induced currents were not observed during application of drugs for longer than 30-s, we concluded that the drugs showed no effect. Data are presented as mean ± SEM. Differences were considered significant when $P < 0.05$ assessed by Student's *t*-test. The normal distribution of the data was evaluated using Jarque-Bera test with a significance level at $P < 0.05$. A Spearman test was used when either data sample lacked a normal distribution.

## RESULTS

*Spontaneous spike activities*

In the measurements with on-cell configuration, about a half of AL neurons exhibited spontaneous spike activities (n = 224/440, 51%). TTX, a selective blocker of voltage-gated $Na^+$ channels, applied at 250 nM abolished the spontaneous spike activities, indicating that this spontaneous activity resulted from action potentials (Fig. 3-1A). Similar results were observed in other 4 neurons. The frequency of the spontaneous firing varied from 0.46 to 17.06 Hz and the mean frequency was 5.26 ± 0.76 Hz ($n$ = 36). The CV values are plotted against firing frequency of each neuron (Fig. 3-1C). In the experiments with whole-cell current clamp recording, 7 out of 10 neurons that had spontaneous firing in the on-cell configuration exhibited spontaneous action potentials (Fig. 3-1B).

*GABA inhibits the spontaneous firing*

GABA at 100 μM was applied to AL neurons that showed spontaneous firing for longer than 5-s in the on-cell configuration (Fig. 3-2A). GABA arrested the spontaneous firing in 7 out of 8 AL neurons tested, and largely inhibited it in one neuron. Summarized data are shown in Fig. 3-2B ($n$ = 8). To identify subtypes of GABA

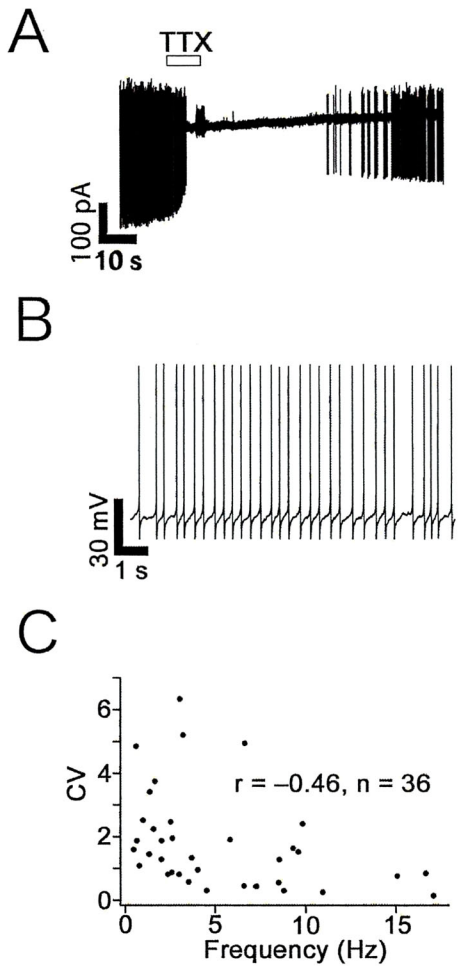


**Fig. 3-1** Spontaneous spikes observed in AL neurons. (A) A typical current trace recorded from an AL neuron in the on-cell configuration is shown. TTX (250 nM) was applied during the period indicated by the open bar. (B) A typical current trace recorded in the whole-cell potential clamp configuration is shown. The AL neuron was dialyzed with the KCl-rich pipette solution and perfused with the normal bath solution. (C) The coefficient of variation (CV) of the spontaneous firing recorded in the on-cell configuration is plotted against the firing frequency ($r = -0.46$, $P < 0.01$ by Speaman test, $n = 36$).

receptors contributing to the inhibition of spontaneous firing, effects of specific GABA agonists were examined. The $GABA_A$ receptor agonist, muscimol, at 100 μM applied for longer than 5 s inhibited spontaneous firing (Figs. 3-2C, D), while the $GABA_B$ receptor agonist, SKF97541, at 100 μM that was applied for longer than 30 s showed no effect on spontaneous firing (Figs. 3-2E, F). From each experiment, the mean firing frequency was calculated before, during and after the drug applications (Figs. 3-2B, D, F).

Effects of antagonists specific to the GABA receptor subtypes were also examined. In neurons showing spontaneous firing in the on-cell configuration, GABA was applied for longer than 5 s in the presence of bicuculline, a $GABA_A$ receptor antagonist, or CGP35348, a $GABA_B$ receptor antagonist. Bicuculline at 50 μM and CGP35348 at 100 μM had no effect on the frequency of spontaneous firing. The application of GABA followed to the application of these two antagonists for longer than 30 s. In the presence of bicuculline, GABA did not reduce the firing frequency ($n = 6$, Fig. 3-3A, B). In contrast, CGP35348 at 100 μM showed no effect on GABA-induced inhibition of spontaneous firing ($n = 5$, Fig. 3-3C, D). These results indicate that GABA inhibits spontaneous firing of AL neurons through activation of $GABA_A$ receptors.

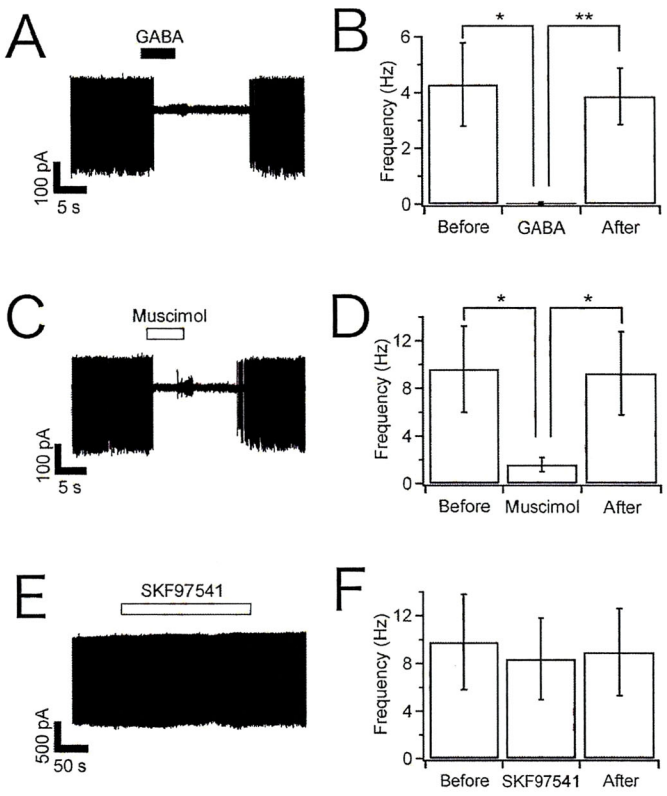


**Fig. 3-2** Effects of GABA and GABA receptor agonists on the spontaneous firing recorded in the on-cell configuration. (A, C, E) Typical current traces recorded from AL neurons in the on-cell configuration are shown. GABA (100 μM), the selective $GABA_A$ agonist muscimol (100 μM) and the selective $GABA_B$ agonist SKF97541 (100 μM) were applied as indicated by the bars. (B, D, F) Effects of GABA ($n$ = 8), muscimol ($n$ = 7) and SKF97541 ($n$ = 6) on spontaneous firing are summarized. The columns and bars indicate the firing frequency before, during and after the application of each drug. *; $P <$ 0.05 and **; $P < 0.01$ by paired Student's $t$-test.

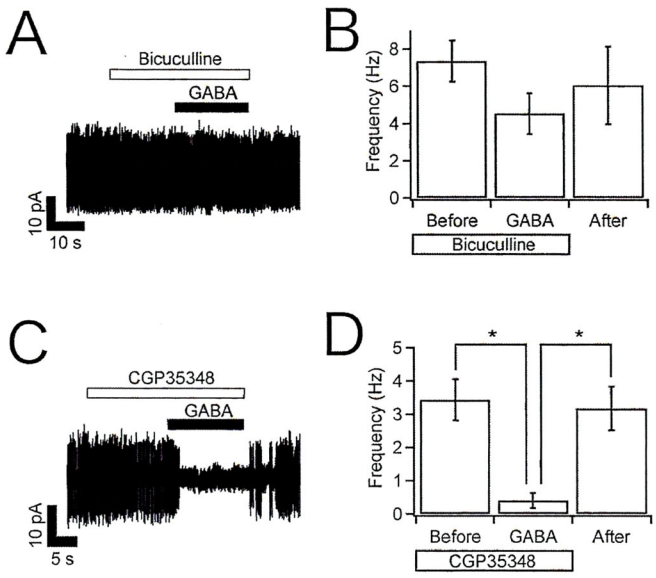


**Fig. 3-3** Effects of GABA receptor antagonists on GABA-induced inhibition of the spontaneous firing recorded in the on-cell configuration. (A, C) Typical current responses to GABA in the presence of the selective $GABA_A$ antagonist bicuculline (50 μM) or the selective $GABA_B$ antagonist CGP35348 (100 μM) are shown. (B, D) Effects of bicuculline ($n = 6$) and CGP35348 ($n = 5$) on the inhibitory action of GABA on spontaneous firing are summarized. The columns and bars indicate the firing frequency before, during and after the application of GABA. *; $P < 0.05$ by paired Student's $t$-test.

*GABA evokes currents carried by $Cl^-$*

To examine whether GABA evokes currents carried by $Cl^-$ through $GABA_A$ receptors, the whole-cell voltage clamp experiments were carried out in AL neurons. In the voltage-clamped neurons dialyzed with the KCl-rich pipette solution, the GABA application evoked a transient inward current when neurons were voltage-clamped at –70 mV (Fig. 3-4). The mean amplitude of GABA-induced currents was 583 ± 115 pA ($n$ = 25). Muscimol (100 μM) also induced a transient inward current and the amplitude was 481 ± 260 pA ($n$ = 5, Fig. 3-4). On the other hand, SKF97541 (100 μM) did not evoke any current ($n$ = 5, Fig. 3-4). We also examined effects of antagonists specific to the GABA receptor subtypes (Fig. 3-5A). Bicuculline at 50 μM greatly reduced amplitudes of GABA-induced currents by 90 ± 9.6 % ($n$ = 9), while CGP35348 at 100 μM did not affect the current amplitudes (Fig. 3-5B). These results suggest that GABA evokes the transient inward current through activation of $GABA_A$ receptors in AL neurons.

To determine the charge-carrying ion of the inward current, GABA at 100 μM was applied to the neurons that were clamped at three different potentials (–70, –50 and –30 mV) in the whole-cell configuration. At each potential, GABA evoked transient inward currents as shown in Fig. 3-6A. Since GABA currents were desensitized during

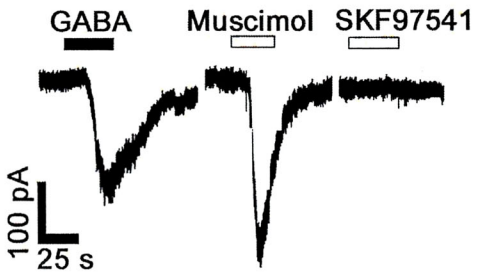


**Fig. 3-4** GABA-induced current responses recorded in the whole-cell configuration. AL neurons were dialyzed with the KCl-rich pipette solution and perfused with the normal bath solution. The membrane potential was clamped at –70 mV. Typical current responses to GABA (100 μM, *a solid bar*), muscimol (100 μM), and SKF97541 (100 μM) applied during the time indicated by the bars.

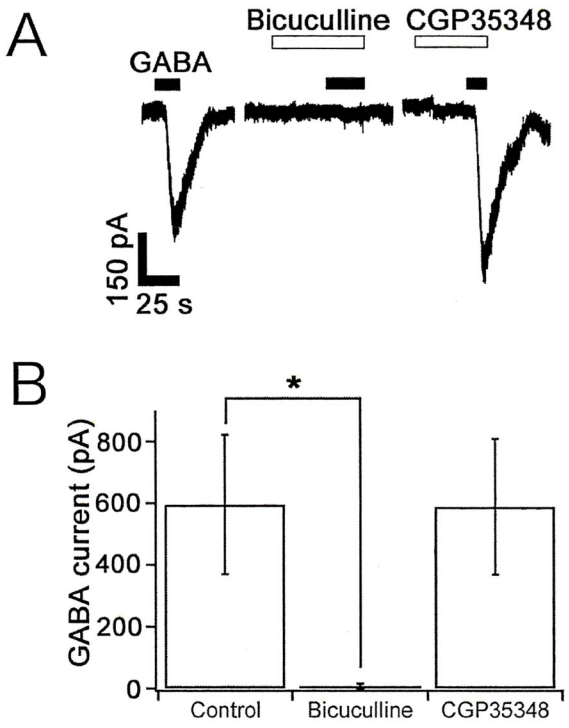


**Fig. 3-5** GABA-induced current responses recorded in the whole-cell configuration. AL neurons were dialyzed with the KCl-rich pipette solution and perfused with the normal bath solution. The membrane potential was clamped at –70 mV. (A) Typical current responses to GABA (*solid bars*) in the absence or presence of the GABA antagonists, bicuculline (50 μM) and CGP97541 (100 μM). The antagonists were applied longer than 30 s before the GABA application and GABA was applied for longer than 5 s as indicated by bars. (B) Inhibitory effects of the GABA receptor antagonists on the GABA-evoked currents were summarized. The columns and bars indicate amplitudes of GABA-evoked inward currents in the absence and presence of bicuculline and CGP35348 ($n = 9$). *; $P < 0.05$ by paired Student's *t*-test.

repetitive applications, current amplitudes at each holding potential (–70, –50, –30 mV) were normalized by the amplitudes of the current evoked by the preceding applications of GABA at a holding potential of –70 mV. Amplitudes of GABA-induced currents increased with an increase in negative holding potentials (Fig. 3-6B). To eliminate the influence of the voltage-gated $K^+$, $Na^+$ and $Ca^{2+}$ channels on the $Cl^-$ currents, neurons were dialyzed with the CsCl-rich pipette solution and perfused with the NMDG-Cl bath solution in the following experiments using a ramp voltage command. Replacement of these cations with NMDG had little or no effect on GABA-induced currents ($n$ = 6, Figs. 3-7A and B). A ramp command from +100 to –100 mV (changing rate: –4 mV/ms) preceded by a steady pulse at +100 mV for 10 ms was applied to neurons before, during and after the application of GABA with an interval of 5 s (Fig. 3-8A). The preceding pulse at +100 mV was applied to obtain I-V relationships of the GABA current under the condition, when voltage-gated $Na^+$ and $Ca^{2+}$ channels were inactivated. The difference current between the currents evoked by the ramp command before and during application of GABA is plotted against the potential of the ramp command in Fig. 3-8B. The intersection potential of these two current responses, i.e. the reversal potential of the GABA current, was –1.3 ± 3.0 mV ($n$ = 6). This value was close to the estimated equilibrium potential for $Cl^-$ that was estimated to be –6.1 mV, indicating that the

GABA current was mainly carried by $Cl^-$, as expected.

*Physiological intracellular $Cl^-$ concentrations in chick embryonic accessory lobe neurons*

Generally, an intracellular concentration of $Cl^-$ ($[Cl^-]_i$) decreases with progress in a development of neurons. In order to know whether activation of $GABA_A$ receptors causes depolarization or hyperpolarization of the membrane, we investigate a physiological $[Cl^-]_i$ in AL neurons by using the gramicidin-perforated patch clamp technique, which do not disrupt native $[Cl^-]_i$ [1]. Figure 3-9 illustrates typical traces of the GABA-evoked currents in a gramicidine-perforated neuron held at –50, –60, and –70mV. GABA evoked an outward current at –50 mV and an inward current at –70 mV, while GABA did not significantly change current level at –60 mV (Fig. 3-9A). Experiments with the ramp command were performed under the same conditions as Fig. 2-8 at the basal holding potential of –70 mV (Fig. 3-9B). The net current evoked by GABA during the ramp command was calculated by subtracting the current before the GABA application from that in the presence of GABA. The amplitude of the net GABA current is plotted against the potentials of the ramp command in Fig. 3-9C. The reversal potential of the GABA-evoked current was estimated to be –61 ± 2.6 mV ($n$ = 3) that is considered to reflect a physiological equilibrium potential for $Cl^-$ in intact neurons.

Assuming that the GABA currents were carried by only $Cl^-$, the estimated $[Cl^-]_i$ using the Nernst equation was 16 ± 1.5 mM ($n$ = 3).

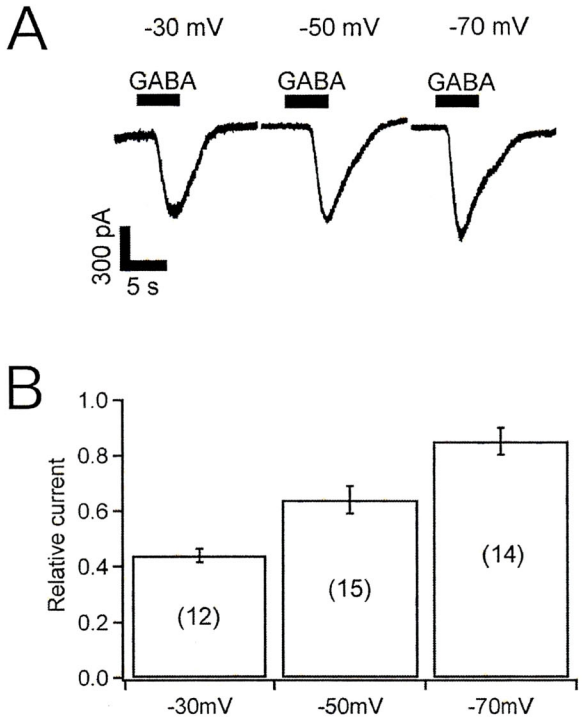


**Fig. 3-6** The Current-voltage relationship of GABA-induced currents. (A) Typical current responses to GABA at 100 μM at holding potentials of –30, –50 and –70 mV recorded in the whole-cell configuration in an AL neuron. (B) Normalized amplitudes of the GABA-evoked inward currents at three different holding potentials are summarized. The current amplitudes were normalized by the amplitudes of the current evoked by preceding application of GABA at a holding potential of –70 mV. The numbers in the bars represent the number of neurons observed.

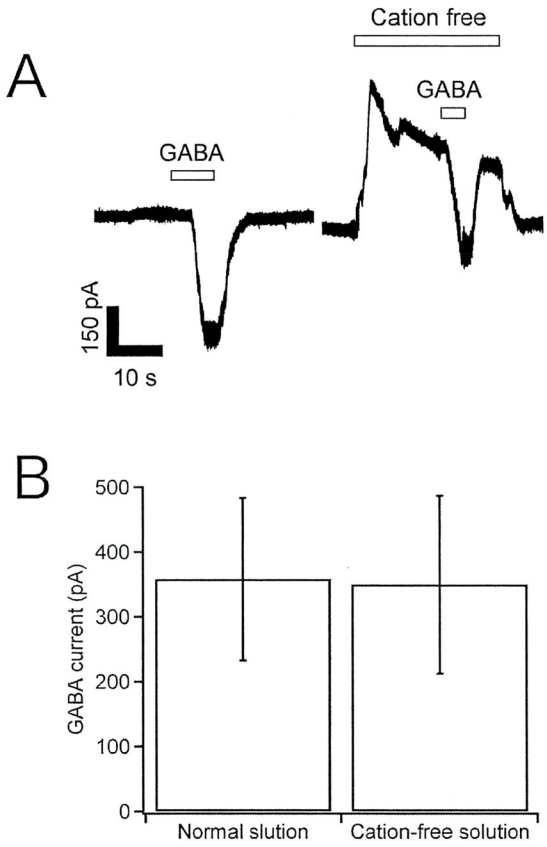


**Fig. 3-7** GABA-induced current responses recorded in the whole-cell configuration. AL neurons were dialyzed with the CsCl-rich pipette solution. The membrane potential was clamped at –70 mV. (A) Typical current responses to GABA at 100 μM perfused with the normal bath solution or cation-free solution. (B) Effects of replacement of $Na^+$, $Ca^{2+}$, and $K^+$ with NMDG in the bath solution on GABA-induced currents are summarized ($n = 6$).

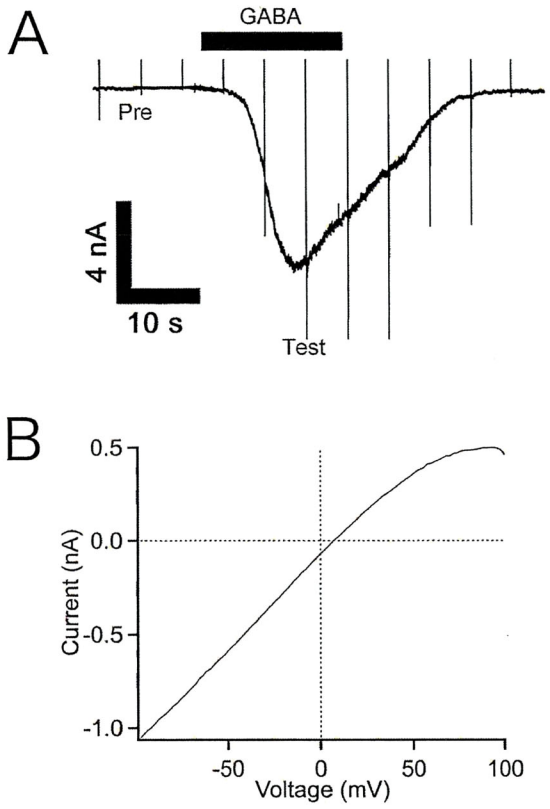


**Fig. 3-8** The current-voltage relationship of GABA-induced currents. (A) A typical response to GABA with the ramp command is shown. A ramp command from +100 to –100 mV (changing rate: –4 mV/ms) preceded by the steady pulse at +100 mV for 10 ms was applied before, during and after the application of GABA. (B) The difference current between the currents evoked by the ramp command before (*Pre* in A) and during (*Test* in A) application of GABA is plotted against the potentials of the ramp command.

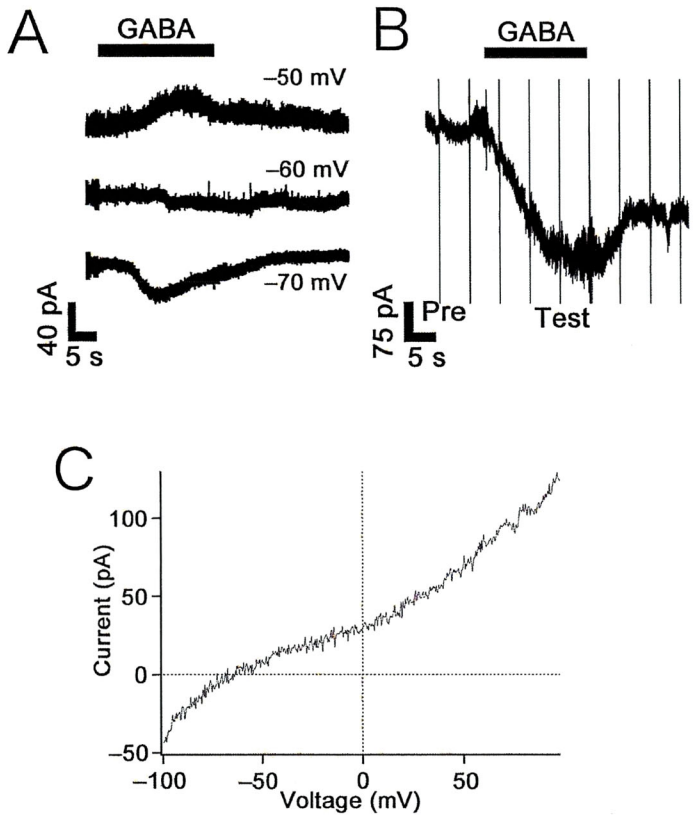


**Fig. 3-9** A reversal potential of the GABA-induced currents recorded in the gramicidin-perforated configuration. (A) Typical traces of GABA currents in an AL neuron held at –50, –60, and –70mV in the gramicidin-perforated configuration. The AL neuron was dialyzed with the KCl-rich pipette solution and perfused with the normal bath solution. (B) A typical response of the GABA-induced current with ramp commands is shown. The ramp command used is as same as in Fig. 3-8. The AL neuron was dialyzed with the CsCl-rich pipette solution and perfused with the NMDG-Cl bath solution and held at –70 mV between the ramp commands. (C) The difference current between the currents evoked by the ramp commands before (*Pre* in B) and during (*Test* in B) application of GABA is plotted against the potentials of the ramp command.

## DISCUSSION

*Spontaneous firing in accessory lobe neurons*

In the present study, we demonstrated that some neurons isolated from chick AL show spontaneous spikes in the on-cell configurations. These spikes were inhibited by 250 nM TTX, indicating that they reflect spontaneous action potentials. It has become clear that AL neurons have an intrinsic mechanism to generate action potentials spontaneously. In the previous study, we did not find the spontaneous firing in AL neurons [45]. The difference in the results between the previous and present study may be caused by the difference in the procedures of the cell isolation. We changed an enzyme to digest AL tissues from trypsin to papain. This change may have made it possible to isolate healthier neurons. There is a correlation between the CV and the firing frequency, i.e. the AL neurons with higher frequencies of firing generate action potentials with a more regular pattern. This is a general characteristic of neurons in other systems [13, 40].

It is known that spontaneous firing has various functions in neurons and neuronal networks. For example, it plays important roles in the maturation of developing nervous systems [5, 12, 22, 26, 43]. Since AL neurons in this study were isolated from embryonic chick, the spontaneous firing observed in this study may support neuronal

development and/or maturation of neuronal networks. On the other hand, chicks can stand up and initiate head movements controlled by the vestibular organ within hours after birth, which are necessary for their survival [6]. The spontaneous firing in chick vestibular tangential principal cells has been reported to appear at birth when chicks start standing, feeding and drinking [44]. It has been also reported that the termination pattern between chick ALs and lamina VIII was already well developed at E18 [10, 11]. In addition to these lines of evidence $[Cl^-]_i$ was low, as estimated to be 16 mM in this study. In mammals, most neurons undergo developmental changes involving changes in $Cl^-$ transporter expression and the equilibrium potential of $Cl^-$, which in turn render GABAergic potentials hyperpolarizing and inhibitory [36]. On the other hand, there is no report about $[Cl^-]_i$ of avian neurons except that of nucleus magnocellularis that has a specialized properties to show the reversal potential of $Cl^-$ around –40 mV [18]. However, since the value of $[Cl^-]_i$ in AL neurons obtained in the present study is low like in matured mammalian neurons, there is a possibility that $K^+$-$Cl^-$ exchangers are well developed in chick AL neurons even at E18-20. Although it is necessary to confirm whether AL neurons of hatched chicks also show spontaneous firing and to compare the characteristics of AL neurons between embryonic and hatched chicks, it is possible that the spontaneous firing of AL neurons have some physiological functions other than

supporting the maturation of neurons and neuronal networks.

It is also known that spontaneous firing plays an important role in neurotransmission of sensory organs. Spontaneous firing in the sensory organs was first described in the study of catfish peripheral nerves [17], and thereafter it has been reported for many first- and second-order sensory neurons [9, 13, 20]. It is proposed that spontaneous firing is essential for the chick vestibular nucleus neurons to transduce incoming vestibular stimuli to vestibulocerebellar neurons, reliably and accurately [8]. Based on the investigations of organs at the lumbosacral region of the bird including ALs, ALs are proposed to be a sensory organ of equilibrium, which is involved in the control of hindlimbs [27, 29-34]. Therefore, the spontaneous firing in AL neurons may have a role as a part of a sensory organ similar to the vestibular nucleus neurons. To confirm this possibility, it is necessary to show that AL neurons sense mechanical signals and the spontaneous firing in AL neurons can be conducted through axons and transmitted to projected neurons.

*GABA receptor subtypes in accessory lobe neurons*

It is reported that AL neurons may have some neurotransmitters and their receptors based on the immunohistochemical evidence [25, 28]. In the present study, we

demonstrated that GABA inhibited the spontaneous firing in AL neurons. This is the first report to show that the AL neurons express functional GABA receptors. Similar inhibition of firing was also observed when neurons were perfused with muscimol or with GABA in combination with CGP35348. In contrast, SKF97541 or GABA in combination with bicuculline did not inhibit the firing. Moreover, in the whole-cell configuration, GABA, muscimol and GABA in combination with CGP35348 but not SKF97541 and GABA in combination with bicuculline evoked the transient currents. The mean reversal potential of GABA-evoked currents was close to the theoretical reversal potential of $Cl^-$. These results indicate that GABA exerts the inhibitory effect on the firing through the activation of the ionotropic $GABA_A$ receptor.

The experiments with the gramicidin-perforated patch clamp technique revealed the physiological reversal potential of the GABA currents in the presence of 167 mM extracellular $Cl^-$. Since $GABA_A$ receptor channels are also permeable to $HCO_3^-$, it is difficult to estimate the exact concentration of $Cl^-$ in the intact neurons. However, since the majority of the charge carrying ions of GABA currents is expected to be $Cl^-$, the approximate $[Cl^-]_i$ and the physiological equilibrium potential are estimated to be 16 mM and –60 mV, respectively. In the previous study, we reported that the voltage-gated $Na^+$ channel in AL neurons were activated at depolarized potentials higher than –50 mV

[45]. Therefore, it is likely that the activation of $GABA_A$ receptors drives the membrane potential to –60 mV and ceases the spontaneous firing in AL neurons.

In many animals, neurons expressing GABA receptors are widely distributed throughout the CNS and the $Cl^-$ current through activated $GABA_A$ receptors is one of the major players to inhibit neurotransmission in the mature CNS [19, 24, 46]. The GABA-induced modulation of the excitability of neurons is important also for the coordinated movements, e.g. walking and swimming. For example, the locomotor central pattern generators of the lamprey that contribute the control of the body movement are modulated by the systems using GABA [14]. It is also shown that the $GABA_A$ receptor modulates the burst frequency of the firing in the locomotor networks of the lamprey [39]. Since AL neurons may have a function to provide coordinated movements, it is important to reveal that electrical activity of AL neurons is inhibited by GABA also in vivo.

## CONCLUDING REMARKS

The series of the studies provides the cell-physiological characteristics of chick AL cells. Chapter 1 shows the first cellular evidence that the functional neurons that can generate complete action potentials exist in the spinal ALs of the chick. Chapter 2 shows chick AL neurons have an intrinsic mechanism to evoke the spontaneous firing and the inhibitory mechanism through the activation of the $GABA_A$ receptor. These results could be further evidence supporting that ALs act as the sensory organ and have a role in keeping body balance in combination with the vertebral canals during walking on the ground.

Although it is evident that VGSC, voltage-gated $K^+$ channels, and $GABA_A$ receptors are expressed in these neurons, further investigations concerning other voltage-gated, ligand-gated ion channels, metabotropic receptors, other excitatory and inhibitory mechanisms, and associated networks are required to clarify the physiological function of avian spinal ALs as sensory organs of equilibrium.

## ACKNOWLEDGEMENTS

I would like to express my sincere gratitude to my supervisor, Dr. Izumi Shibuya, Professor, Department of Veterinary Medicine, Faculty of Agriculture, Tottori University, Japan, for providing me this precious study opportunity as a Ph.D student in his laboratory.

I especially would also like to express my deepest appreciation to my supervisor, Dr. Naoki Kitamura, Associate professor, Department of Veterinary Medicine, Faculty of Agriculture, Tottori University, Japan, for his elaborated guidance, considerable encouragement and invaluable discussion that make my research of great achievement and my study life unforgettable.

I sincerely wish to appreciate Dr. Noboru Murakami, Professor, Department of Veterinary Physiology, Faculty of Agriculture, Miyazaki University, Japan, Dr. Tomohiro Imagawa, Professor, Department of Veterinary Image Diagnosis, Faculty of Agriculture, Tottori University, Japan, and Dr. Kenji Takahashi, Associate professor, Department of Veterinary Pharmacology, Faculty of Agriculture, Tottori University Japan, for their intimate advice and comments to my research projects and thesis.

I am very grateful also to Hikaru Shinohara, Kagoshima prefecture; Keita Takahashi, Kudo Animal Hospital (Okinawa, Japan) and the students in this laboratory for their

valuable cooperation in my experiments.

This study was supported by a research grant from the President of Tottori University, KAKENHI (Grant #: 16780200, 18380175), and Grant-in-Aid for JSPS Fellows.

I would like to extend my indebtedness to my family for their endless love, understanding, support, encouragement and sacrifice throughout my study.

Finally, I would like to thank and pay my respects to animals for giving excellent data in my study.

## Reference


[1] N. Akaike, Gramicidin perforated patch recording and intracellular chloride activity in excitable cells, Prog Biophys Mol Biol 65 (1996) 251-264.

[2] M. Antal, Z. Puskár, A. Birinyi, J. Storm-Mathisen, Development, neurochemical properties, and axonal projections of a population of last-order premotor interneurons in the white matter of the chick lumbosacral spinal cord, J Exp Zool 286 (2000) 157-172.

[3] M. Biederman-Thorson, J. Thorson, Rotation-compensating reflexes independent of the labyrinth and the eye., J Comp physiol 83 (1973) 103-122.

[4] A. Birinyi, K. Viszokay, I. Weber, O. Kiehn, M. Antal, Synaptic targets of commissural interneurons in the lumbar spinal cord of neonatal rats, J Comp Neurol 461 (2003) 429-440.

[5] N. Chub, M.J. O'Donovan, Blockade and recovery of spontaneous rhythmic activity after application of neurotransmitter antagonists to spinal networks of the chick embryo, J Neurosci 18 (1998) 294-306.

[6] J.D. Decker, The influence of early extirpation of the otocysts on development of behavior of the chick, J Exp Zool 174 (1970) 349-363.

[7] J. Delius, W. Vollrath, Rotation conpensating reflexes independent of the

labyrinth., J Comp Physiol 83 (1973) 123-134.

[8] S. du Lac, S.G. Lisberger, Cellular processing of temporal information in medial vestibular nucleus neurons, J Neurosci 15 (1995) 8000-8010.

[9] S. du Lac, S.G. Lisberger, Eye movements and brainstem neuronal responses evoked by cerebellar and vestibular stimulation in chicks, J Comp Physiol A 171 (1992) 629-638.

[10] A.L. Eide, The axonal projections of the Hofmann nuclei in the spinal cord of the late stage chicken embryo, Anat Embryol (Berl) 193 (1996) 543-557.

[11] A.L. Eide, J.C. Glover, Development of an identified spinal commissural interneuron population in an amniote: neurons of the avian Hofmann nuclei, J Neurosci 16 (1996) 5749-5761.

[12] B. Fedirchuk, P. Wenner, P.J. Whelan, S. Ho, J. Tabak, M.J. O'Donovan, Spontaneous network activity transiently depresses synaptic transmission in the embryonic chick spinal cord, J Neurosci 19 (1999) 2102-2112.

[13] J.M. Goldberg, C. Fernandez, Physiology of peripheral neurons innervating semicircular canals of the squirrel monkey. I. Resting discharge and response to constant angular accelerations., J Neurophysiol 34 (1971) 26.

[14] S. Grillner, The motor infrastructure: from ion channels to neuronal networks,

Nat Rev Neurosci 4 (2003) 573-586.

[15] I. Hammar, B.A. Bannatyne, D.J. Maxwell, S.A. Edgley, E. Jankowska, The actions of monoamines and distribution of noradrenergic and serotoninergic contacts on different subpopulations of commissural interneurons in the cat spinal cord, Eur J Neurosci 19 (2004) 1305-1316.

[16] P.J. Harrison, E. Jankowska, D. Zytnicki, Lamina VIII interneurones interposed in crossed reflex pathways in the cat, J Physiol 371 (1986) 147-166.

[17] H. Hoagland, Impulses from Sensory Nerves of Catfish, Proc Natl Acad Sci USA 18 (1932) 701-705.

[18] M.A. Howard, R.M. Burger, E.W. Rubel, A developmental switch to GABAergic inhibition dependent on increases in Kv1-type $K^+$ currents, J Neurosci 27 (2007) 2112-2123.

[19] R.L. Hyson, A.D. Reyes, E.W. Rubel, A depolarizing inhibitory response to GABA in brainstem auditory neurons of the chick, Brain Res 677 (1995) 117-126.

[20] T.A. Jones, S.M. Jones, Spontaneous activity in the statoacoustic ganglion of the chicken embryo, J Neurophysiol 83 (2000) 1452-1468.

[21] A. Kölliker, Über die oberflächlichen Nervenkerne im Marke der Vögel und

Reptilien. , Z Wiss Zool 72 (1902) 126-180.

[22] L.C. Katz, C.J. Shatz, Synaptic activity and the construction of cortical circuits, Science 274 (1996) 1133-1138.

[23] S. Masetto, M. Bosica, M.J. Correia, O.P. Ottersen, G. Zucca, P. Perin, P. Valli, $Na^+$ currents in vestibular type I and type II hair cells of the embryo and adult chicken, J Neurophysiol 90 (2003) 1266-1278.

[24] C.J. McBain, A. Fisahn, Interneurons unbound, Nat Rev Neurosci 2 (2001) 11-23.

[25] T. Milinski, R. Necker, Histochemical and immunocytochemical investigations of the marginal nuclei in the spinal cord of pigeons (*Columba livia*), Brain Res Bull 56 (2001) 15-21.

[26] L.D. Milner, L.T. Landmesser, Cholinergic and GABAergic inputs drive patterned spontaneous motoneuron activity before target contact, J Neurosci 19 (1999) 3007-3022.

[27] R. Necker, Are paragriseal cells in the avian lumbosacral spinal cord displaced ventral spinocerebellar tract neurons?, Neurosci Lett 382 (2005) 56-60.

[28] R. Necker, Histological and immunocytochemical characterization of neurons located in the white matter of the spinal cord of the pigeon, J Chem Neuroanat

27 (2004) 109-117.

[29] R. Necker, Mechanosensitivity of spinal accessory lobe neurons in the pigeon, Neurosci Lett 320 (2002) 53-56.

[30] R. Necker, Projections of the marginal nuclei in the spinal cord of the pigeon, J Comp Neurol 377 (1997) 95-104.

[31] R. Necker, Specializations in the lumbosacral spinal cord of birds: morphological and behavioural evidence for a sense of equilibrium, Eur J Morphol 37 (1999) 211-214.

[32] R. Necker, Specializations in the lumbosacral vertebral canal and spinal cord of birds: evidence of a function as a sense organ which is involved in the control of walking, J Comp Physiol A Neuroethol Sens Neural Behav Physiol 192 (2006) 439-448.

[33] R. Necker, The structure and development of avian lumbosacral specializations of the vertebral canal and the spinal cord with special reference to a possible function as a sense organ of equilibrium, Anat Embryol (Berl) 210 (2005) 59-74.

[34] R. Necker, A. Janßen, T. Beissenhirtz, Behavioral evidence of the role of lumbosacral anatomical specializations in pigeons in maintaining balance during terrestrial locomotion, J Comp Physiol A 186 (2000) 409-412.

[35] G. Orlovsky, T. Deliagina, S. Grillner, Neuronal control of locomotion. From mollusc to man., Oxford University Press Oxford (1999) 322.

[36] C. Rivera, J. Voipio, J.A. Payne, E. Ruusuvuori, H. Lahtinen, K. Lamsa, U. Pirvola, M. Saarma, K. Kaila, The $K^+/Cl^-$ co-transporter KCC2 renders GABA hyperpolarizing during neuronal maturation, Nature 397 (1999) 251-255.

[37] J. Rosenberg, R. Necker, Fine structural evidence of mechanoreception in spinal lumbosacral accessory lobes of pigeons, Neurosci Lett 285 (2000) 13-16.

[38] J. Rosenberg, R. Necker, Ultrastructural characterization of the accessory lobes of Lachi in the lumbosacral spinal cord of the pigeon with special reference to intrinsic mechanoreceptors, J Comp Neurol 447 (2002) 274-285.

[39] D.E. Schmitt, R.H. Hill, S. Grillner, The spinal GABAergic system is a strong modulator of burst frequency in the lamprey locomotor network, J Neurophysiol 92 (2004) 2357-2367.

[40] M. Shao, J.C. Hirsch, K.D. Peusner, Maturation of firing pattern in chick vestibular nucleus neurons, Neuroscience 141 (2006) 711-726.

[41] M.R. Smith, R.D. Smith, N.W. Plummer, M.H. Meisler, A.L. Goldin, Functional analysis of the mouse Scn8a sodium channel, J Neurosci 18 (1998) 6093-6102.

[42] R.D. Smith, A.L. Goldin, Functional analysis of the rat I sodium channel in

xenopus oocytes, J Neurosci 18 (1998) 811-820.

[43] J. Tabak, W. Senn, M.J. O'Donovan, J. Rinzel, Modeling of spontaneous activity in developing spinal cord using activity-dependent depression in an excitatory network, J Neurosci 20 (2000) 3041-3056.

[44] J. Wallman, J. Velez, B. Weinstein, A.E. Green, Avian vestibuloocular reflex: adaptive plasticity and developmental changes, J Neurophysiol 48 (1982) 952-967.

[45] Y. Yamanaka, N. Kitamura, I. Shibuya, Chick spinal accessory lobes contain functional neurons expressing voltagegated sodium channels generating action potentials, Biomed Res 29 (2008) 205-211.

[46] C.X. Yang, H. Xu, K.Q. Zhou, M.Y. Wang, T.L. Xu, Modulation of gamma-aminobutyric acid A receptor function by thiopental in the rat spinal dorsal horn neurons, Anesth Analg 102 (2006) 1114-1120.

## SUMMARY

**【INTRODUCTION・PURPOSE】** In the avian spinal cord, ten pairs of protrusions, called accessory lobes (ALs), are present at both lateral sides of the lumbosacral spinal cord near the dentate ligaments. Morphological and histological information about ALs suggests that ALs act as a sensory organ and have a role in keeping body balance in combination with the vertebral canals during walking on the ground. It was also reported that neurons located in an outer layer of ALs showed GABA- and glutamic acid decarboxylase (GAD)-like immunoreactivity more strongly than centrally located neurons, which were surrounded by the GAD-immunoreactive terminals. Although there have been much experimental data to suggest that ALs in birds act as the sensory organ, there is little evidence to indicate that cells in ALs have a neuronal function, and there is no information about cell-physiological features of AL cells. To elucidate these points, we developed a method to dissociate cells from chick ALs and made electrophysiological recordings by the patch clamp technique.

**【RESULTS・DISCUSSION】** There are two types of cells in chick ALs; one is a cell with rich and the other is a cell with clear cytosolic structure. Considering that AL consists of glycogen cells, derived from astroglial cells, and neurons, the dissociated cells with the clear cytosol, which no voltage-gated ionic currents may be glycogen cells.

In contrast, the other type of cells with the rich cytosolic structures showed voltage-gated currents, indicating that they express functional voltage-gated $Na^+$ channels (VGSCs) and voltage-gated $K^+$ channels. Moreover, these cells generate full action potentials. These results clearly indicate that the cells with rich cytosolic structures are functional neurons. Acutely dissociated chick AL cells with the clear cytoplasma often had short processes, and cells with rich cytosolic structures sometimes had some dendrites or axons with many branches. Such morphology is consistent with the reported properties of the glycogen cells and neurons respectively in pigeon ALs.

About 50 % of neurons isolated from chick AL showed spontaneous firing in the on-cell configuration. It has become clear that AL neurons have an intrinsic mechanism to generate action potentials spontaneously. It is proposed that spontaneous firing is essential for the chick vestibular nucleus neurons to transduce incoming vestibular stimuli to vestibulocerebellar neurons, reliably and accurately. Therefore, the spontaneous firing found in AL neurons may have a role as a part of a sensory organ similar to the vestibular nucleus neurons.

The present study also demonstrated that GABA inhibited the spontaneous firing in AL neurons. This result coincides with the immunohistochemical evidence that GABA-containing nerve terminals surround AL neurons. The experiments using

pharmacological tools to analysis GABA receptors in this study explain that, in AL neurons, GABA exerts the inhibitory effect on the firing through the activation of the ionotropic $GABA_A$ receptor. In addition, the experiments with the gramicidin-perforated patch clamp technique revealed that the physiological equilibrium potential is about –60 mV. Considering that the VGSCs in AL neurons were activated at more depolarized potentials than –50 mV, it seems that the activation of $GABA_A$ receptors drives the membrane potential to –60 mV and ceases the spontaneous firing in AL neurons. In mammals, most neurons undergo developmental changes involving changes in $Cl^-$ transporter expression and the equilibrium potential of $Cl^-$, which in turn render GABAergic potentials hyperpolarizing and inhibitory. On the other hand, there is little information about avian neurons in this field. However, since the value of $[Cl^-]_i$ in AL neurons obtained in the present study is low like in matured mammalian neurons, there is a possibility that $K^+$-$Cl^-$ exchangers are well developed in chick AL neurons even at E18-20.

In many animals, neurons expressing GABA receptors are widely distributed throughout the CNS and the $Cl^-$ current through activated $GABA_A$ receptors is one of the most major players to inhibit neurotransmission in the mature CNS. The GABA-induced modulation of the excitability of neurons is important also for the

coordinated movements, e.g. walking and swimming. For example, the locomotor central pattern generators of the lamprey that contribute the control of the body movement are modulated by the systems using GABA. Since AL neurons may have a function to provide coordinated movements, it is important to reveal that electrical activity of AL neurons is inhibited by GABA also *in vivo*.

**【CONCLUSION】** Chick ALs have functional neurons, which have an intrinsic mechanism to evoke the spontaneous action potentials and the inhibitory mechanism through the activation of the $GABA_A$ receptor. It seems that these results support the hypothesis; ALs in birds can act as the sensory organs.